European Journal of Cardio-Thoracic Surgery Advance Access published November 24, 2014

European Journal of Cardio-Thoracic Surgery (2014) 1–11
doi:10.1093/ejcts/ezu428

ORIGINAL ARTICLE

BASIC SCIENCE

Alteration of inflammatory response by shock wave therapy leads to reduced calcification of decellularized aortic xenografts in mice†

Can Tepeköylü[a,b], Daniela Lobenwein[a], Stefan Blunder[c], Radoslaw Kozaryn[a], Marion Dietl[a], Paul Ritschl[d], Elisabeth J. Pechriggl[b], Michael J.F. Blumer[b], Mario Bitsche[b], Roland Schistek[a], Katja Kotsch[d], Helga Fritsch[b], Michael Grimm[a] and Johannes Holfeld[a,*]

[a] University Hospital for Cardiac Surgery, Medical University of Innsbruck, Innsbruck, Austria
[b] Division of Clinical and Functional Anatomy, Department of Anatomy, Histology and Embryology, Medical University of Innsbruck, Innsbruck, Austria
[c] University Hospital for Dermatology and Venerology, Medical University of Innsbruck, Innsbruck, Austria
[d] University Hospital for Visceral, Transplant and Thoracic Surgery, Medical University of Innsbruck, Innsbruck, Austria

* Corresponding author. Department of Cardiac Surgery, Medical University of Innsbruck, Anichstraße 35, 6020 Innsbruck, Austria, Tel: +43-512-50480800; fax: +43-512-50422528; e-mail: johannes.holfeld@i-med.ac.at (J. Holfeld).

Received 20 June 2014; received in revised form 2 October 2014; accepted 16 October 2014

Abstract

OBJECTIVES: Tissue-engineered xenografts represent a promising treatment option in heart valve disease. However, inflammatory response leading to graft failure and incomplete *in vitro* repopulation with recipient cells remain challenging. Shock waves (SWs) were shown to modulate inflammation and to enhance re-epithelialization. We therefore aimed to investigate whether SWs could serve as a feasible adjunct to tissue engineering.

METHODS: Porcine aortic pieces were decellularized using sodium deoxycholate and sodium dodecylsulphate and implanted subcutaneously into C57BL/6 mice ($n = 6$ per group). The treatment (shock wave therapy, SWT) group received SWs (0.1 mJ/mm^2, 500 impulses, 5 Hz) for modulation of inflammatory response directly after implantation; control animals remained untreated (CTR). Grafts were harvested 72 h and 3 weeks after implantation and analysed for inflammatory cytokines, macrophage infiltration and polarization, osteoclastic activity and calcification. Transmission electron microscopy (TEM) was performed. Endothelial cells (ECs) were treated with SWs and analysed for macrophage regulatory cytokines. In an *ex vivo* experimental set-up, decellularized porcine aortic valve conduits were reseeded with ECs with and without SWT (0.1 mJ/mm^2, 300 impulses, 3 Hz), fibroblasts as well as peripheral blood mononuclear cells (all human) and tested in a pulsatile flow perfusion system for cell coverage.

RESULTS: Treated ECs showed an increase of macrophage migration inhibitory factor and macrophage inflammatory protein 1β, whereas CD40 ligand and complement component C5/C5a were decreased. Subcutaneously implanted grafts showed increased mRNA levels of tumour necrosis factor α and interleukin 6 in the treatment group. Enhanced repopulation with recipient cells could be observed after SWT. Augmented macrophage infiltration and increased polarization towards M2 macrophages was observed in treated animals. Enhanced recruitment of osteoclastic cells in proximity to calcified tissue was found after SWT. Consequently, SWT resulted in decreased areas of calcification in treated animals. The reseeding experiment revealed that fibroblasts showed the best coverage compared with other cell types. Moreover, SW-treated ECs exhibited enhanced repopulation compared with untreated controls.

CONCLUSIONS: SWs reduce the calcification of subcutaneously implanted decellularized xenografts via the modulation of the acute macrophage-mediated inflammatory response and improves the *in vitro* repopulation of decellularized grafts. It may therefore serve as a feasible adjunct to heart valve tissue engineering.

Keywords: Heart valve disease • Tissue engineering • Shock wave therapy • Macrophages • Decellularized xenografts

INTRODUCTION

Heart valve disease is one of the most frequent indications for cardiac surgery, with aortic valve stenosis as the main underlying pathology. Currently, either mechanical or biological prostheses are used for replacement in clinical routine, both of which have distinct limitations. Mechanical heart valves have a nearly infinite life span, but require life-long anticoagulation treatment including all its risks [1]. Bioprostheses do not require anticoagulation treatment and show better haemodynamic properties than mechanical prostheses. However, glutaraldehyde fixation results in limited lifespan due to progressive degeneration that may lead to structural failure and reoperation [2].

Tissue engineering approaches aim to replicate native valves, thus overcoming the limitations of existing valve prostheses [3]. To

† Presented at the European Society of Cardiology (ESC) Congress, Barcelona, Spain, 30 August 2014.

achieve these requirements, tissue-engineered heart valves should exhibit mechanical durability, not trigger thrombogenic and/or immunogenic reactions and be adequately repopulated with recipient cells to obtain a living valve that can grow, repair and remodel [4]. Thereby, an acellular matrix serving as a 3D guiding structure for repopulating cells is obtained from either synthetic biodegradable polymers or from xenogenic or allogenic valve tissue by decellularization [5, 6]. Matrices and decellularized valves or conduits have been implanted without preseeding and have shown the ability for reseeding *in vivo* [7]. Other approaches include preseeding of the matrices prior to implantation with cells obtained from the recipient and allowed to mature *in vitro* under physiological conditions [5]. The superiority of one of all these approaches is still not fully clarified.

In the field of heart valve engineering, the use of decellularized xenografts has been described as a promising approach. The removal of cellular components markedly reduces the antigenicity of xenogenic heart valves [8]. First encouraging results have been reported in preclinical as well as in clinical trials [9, 10].

However, even after successful cell removal, decellularized grafts can trigger immune reactions as well as thrombogenic events, resulting in graft failure [11]. Remaining antigens attract proinflammatory immune cells [8]. The inflammatory response upon implanted tissue-engineered heart valves can lead to early graft failure or chronic graft degeneration, both of which can have detrimental consequences for patients as shown in the SYNERGRAFT trial [11].

The immune system plays a pivotal role in the degeneration of tissue-engineered xenografts [11]. Macrophages reportedly orchestrate the early inflammatory response following implantation of acellular biomatrices [12]. Their recruitment and survival are enhanced by tumour necrosis factor α (TNF-α) via TNF-α receptor 1 and 2 and by interleukin 6 (IL-6) via the signal transducer and activator of transcription 3 pathway [13, 14]. However, exact mechanisms of acute graft failure and chronic graft degeneration remain largely unknown.

In addition to the acute inflammatory response upon graft implantation, insufficient repopulation with recipient cells prior to implantation represents a major challenge for tissue engineering [15].

Shock wave therapy (SWT) has been reported to positively influence inflammation, to induce tissue regeneration and to enhance re-epithelialization in cutaneous burn wounds [16–18]. In doing so, no damage of treated tissue has been observed [19]. We therefore hypothesized that the effect of modulating inflammation and stimulating re-epithelializtaion could serve as a feasible adjunct to tissue engineering of heart valves. This study therefore aims to investigate whether (i) the modulation of the acute, macrophage-mediated inflammatory response to decellularized xenografts may beneficially influence the chronic inflammatory degeneration process and thus delay graft degeneration and (ii) the described effect of increased re-epithelialization upon SWT could positively influence graft reseeding.

To address the first hypothesis, decellularized xenografts were implanted subcutaneously in mice. Immediately after implantation, the tissue surrounding the decellularized xenograft was treated with shock waves (SWs). In a second experiment, reseeded decellularized porcine aortic valve conduits were implanted into a bioreactor under pulsatile flow conditions and treated with SWs.

MATERIALS AND METHODS

Grafts and decellularization

Porcine aortas from domestic pigs were obtained from a local slaughterhouse and decellularized as described previously [6]. Briefly, aortas were placed in 0.5% sodium deoxycholate (Sigma, St Louis, MO, USA)/0.5% sodium dodecylsulphate (Sigma) for 24 h. Subsequently, six wash cycles of 12 h each [phosphate-buffered saline (PBS) with penicillin and streptomycin (P/S), 100 mg/ml, Sigma] followed for the removal of remaining decellularization agents and cell debris. Successful decellularization was confirmed in haematoxylin–eosin (HE) stainings as described previously [6].

For the subcutaneous implantation model, pieces of the ascending aortic wall were obtained. A specifically designed biopsy punch of 0.5 cm × 0.5 cm was used to guarantee the exact same size among the samples. Explanted specimens were divided into three parts, and used for RNA extraction, cryosections or paraffin sections. For the bioreactor reseeding experiment, aortic valve conduits were obtained from the decellularized porcine aortas. After harvesting, specimens were used for paraffin sections.

Biomechanical testing

Transversal and longitudinal strips were excised from native and decellularized porcine aortic walls. A specifically designed biopsy punch was used to guarantee the exact same size among all samples. The dog-bone shaped specimens had a width of 10 mm at the mounting site and a width of 5 mm at the test site. They were fixed with clamps on both sides and slowly elongated with a custom-made extension machine within 120 s. The tension force was continuously measured by a PCE FM 50 Tensiometer (PCE Germany Corporation, Meschede, Germany) and transferred by a data-logging software every second to a computer chart. The force (in newton) at which the rupture occurred was compared between the groups. For better evaluation of stiffness, the Young's modulus (=tensile modulus) was calculated according to the formula $E = (\sigma/\varepsilon) = (F/A)/(\Delta l/l_0)$. Results were calculated in N/mm^2.

Animal experiments

The experiments were approved by the institutional animal care and use committee at Innsbruck Medical University and by the Austrian ministry of science. The investigation conformed to the 'Guide for the Care and Use of Laboratory Animals' published by the US National Institutes of Health (NIH Publication No. 85–23, revised 1996; available from: www.nap.edu/catalog/5140.html). Male 12- to 14-week old C57BL/6 mice were obtained from Charles River laboratories (Wilmington, MA, USA) and randomly divided into four groups. The SW group received SWT immediately after subcutaneous graft implantation (SWT), whereas control animals were left untreated (CTR). Animals were sacrificed at two time points (72 h and 3 weeks after implantation), resulting in a total of four groups, $n = 6$.

Subcutaneous implantation model

Subcutaneous implantation was performed as described elsewhere [20]. Briefly, animals were anaesthetized by an intraperitoneal injection of ketamine (80–100 mg/kg BW) and xylazin (5–10 mg/kg BW). Subsequently, a dorsal skin incision of ∼1.5 cm was made. Skin was dissected from subcutaneous tissue. Two subcutaneous slots per animal were formed. In every subcutaneous slot, a small piece of decellularized porcine aorta of 0.5 cm × 0.5 cm was inserted. Skin incisions were closed with a single-knot suture. Tissue was explanted 72 h and 3 weeks after implantation and divided

into three parts. One part was shock-frozen in liquid nitrogen for RNA extraction and subsequent RT-PCR analysis, one part was fixed with formaldehyde and embedded in paraffin and one part was embedded in optimal cutting temperature (OCT) compound (TISSUE-TEK®, Sakura Finetek, Netherlands) for cryosections.

Shock wave treatment

SWT was applied as described previously [21]. Briefly, the Orthogold device with applicator CG050-P (TRT LLC, Tissue Regeneration Technologies, Woodstock, GA, USA) was used. Then 500 impulses per mouse were applied at an energy flux density of 0.1 mJ/mm^2 and a frequency of 5 Hz. Common ultrasound gel was used for coupling. The treatment was performed immediately after implantation of the grafts while animals were still under anaesthesia. Thereby, SWs were focused to the site of implantation for treatment of the tissue surrounding the implanted graft.

Reverse transcription–polymerase chain reaction

Six animals per group and two grafts per animal were analysed. Total RNA was extracted from homogenized tissue using the RNAII Kit (Machery-Nagel; Düren, Germany) according to the manufacturer's instructions. Real-time reverse transcription–polymerase chain reaction (RT-PCR) for gene expression analysis was performed with the ABI PRISM 7500 Sequence Detection System (Applied Biosystems, Life Technologies, Carlsbad, CA, USA). Primers for TNFa 5′ TCG AGT GAC AAG CCC GTA GC 3′ (S); 5′ CTC AGC CAC TCC AGC TGC TC 3′ (AS); 5′ CGT CGT AGC AAA CCA CCA AGC GGA 3′ (probe) and IL-6 5′ TCC AGA AAC CGC TAT GAA GTT CC 3′ (S); 5′ GTC ACC AGC ATC AGT CCC AAG 3′ (AS); 5′ CTC TGC AAG AGA CTT CCA TCC AGT TGC CT3′ (probe) were designed using Primer Express Software (Applied Biosystems). The PCR reaction was performed in a final volume of 25 µl containing 1 µl of cDNA, 12.5 µl of Master Mix (Applied Biosystems), 1 µl of fluorogenic hybridization probe, 6 µl of primer mix and 5.5 µl of distilled water. The amplification consisted of a two-step PCR (40 cycles; 15-s denaturation step at 95°C and 1-min annealing/extension step at 60°C). Specific gene expression was normalized to the housekeeping gene beta-actin given by the formula $2_t^{-\Delta C}$. The result for the relative gene expression was calculated by the 2-DDCt method. The mean C_t values were calculated from double determinations and samples were considered negative if the C_t values exceeded 40 cycles. Results are shown as relative gene expression.

Histological analysis and immunofluorescence

Grafts were harvested 72 h and 3 weeks after implantation. For all histological analyses, six animals per group and two grafts per animal were analysed. Grafts were fixed in 10% (v/v) buffered formaldehyde, dehydrated with graded ethanol series and embedded in paraffin. For immunofluorescence analysis, fresh tissue was embedded in OCT compound (TISSUE-TEK®) and snap-frozen in liquid nitrogen. Serial transverse sections of 5 µm were cut and subsequently mounted on slides. HE staining was performed. For cell invasion analysis, five HE-stained slides per explanted graft were investigated. Three random areas per slide were photographed and analysed by a single, blinded researcher. Cell nuclei were counted and divided by the imaged area. Cell counting as well as area measurement was accomplished using ImageJ software (National Institutes of Health, Bethesda, MD, USA). Macrophages were identified using rat monoclonal anti-F4/80 antibody (Abcam, Cambridge, UK). Rabbit polyclonal anti-CD163 was used for the identification of M2 macrophages (Bioss Antibodies, Woburn, MA, USA). Alexa Fluor® 568 goat anti-rat antibody and Alexa Fluor® 488 goat anti-rabbit antibody (both Life Technologies) served as secondary antibodies, whereas nuclei were stained with 4′,6-diamidino-2-phenylindole (Life Technologies). Again, five slides per explanted graft were investigated. Three random areas per slide were photographed and analysed. The total number of F4/80-positive cells was related to the total number of nuclei per high-power field. Cell counting was accomplished using ImageJ software (National Institutes of Health). Sections were examined with a Zeiss Axioplan 2 (Zeiss, Oberkochen, Germany) and photographed as colour images using a Zeiss AxioCam HR and AxioVision 4.1. software (Zeiss).

Enzyme histochemistry

For the analysis of tartrate-resistant acid phosphatase (TRAP) activity sections were deparaffinized, rinsed in PBS and incubated with a solution containing 50 mM sodium acetate (pH 5.2), 0.15% naphthol-AS-TR-phosphate, 50 mM sodium tartrate and 0.1% Fast Red T.R. (Sigma Aldrich Chemie GmbH, Taufkirchen, Germany) for up to 1 h at room temperature. Subsequently, the sections were rinsed in PBS and counterstained with toluidine blue for 1 min at room temperature. Six animals per group and two aortic specimens per animal were examined. Five slides per explanted specimen were analysed. On every slide, the total number of TRAP-positive cells was counted using ImageJ software (National Institutes of Health). A mean value per explanted graft was calculated. Sections were examined with a Zeiss Axioplan 2 (Zeiss) and photographed as colour images using a Zeiss AxioCam HR and AxioVision 4.1. software (Zeiss).

Von Kossa

Paraffin-embedded tissue sections were analysed for calcification using von Kossa staining. For this purpose, a commercially available staining kit (Merck Millipore, Billerica, MA, USA) was purchased. The staining was performed as suggested by the manufacturer. Again, five slides per harvested graft were analysed. On every slide, the total calcified area was quantified using ImageJ software (National Institutes of Health). A mean value per explanted graft was calculated. Results are represented as arbitrary units. Sections were examined with a Zeiss Axioplan 2 (Zeiss) and photographed as colour images using a Zeiss AxioCam HR and AxioVision 4.1. software (Zeiss). Serial sections of TRAP and von Kossa stainings were merged using Adobe Photoshop 5.0 Software (Adobe Systems, San Jose, CA, USA).

Light microscopy and transmission electron microscopy

Tissue samples were fixed in 2.5% glutaraldehyde and 2% paraformaldehyde buffered in sodium cacodylate (0.1 M, pH = 7.4) overnight at 4°C. Subsequently, they were rinsed in sodium cacodylate buffer and post-fixed in 1% osmium tetroxide in distilled water for

3–4 h at 4°C. Again, samples were rinsed in buffer and dehydrated in graded ethanol series and 100% acetone. Finally, they were embedded in EPON resin. Semithin sections (1 µm) were cut on a Reichert Ultracut S microtome (Leica Microsystem, Wetzlar, Germany) with a histo-jumbo-diamond knife (Diatome, Biel, Switzerland) and stained with toluidine blue (1% toluidine blue, 1% borax in distilled water) for 20 s at 60°C. Ultrathin sections (90 nm) were cut on the same microtome with an ultra-diamond knife, mounted on dioxan-formvar-coated copper slot-grids (# G2500C, Christine Gröpl Elektronenmikroskopie, Tulln, Austria) and stained with uranyl acetate and lead citrate (Leica Ultrostainer, Leica Microsystem). The semithin sections were examined with a Zeiss Axioplan 2 (Zeiss) and photographed as colour images using a Zeiss AxioCam HR and AxioVision 4.1. software (Zeiss).The ultrathin sections were examined with a Philips CM 120 transmission electron microscope at 80 kV (FEI, Eindhoven, Netherlands) equipped with a MORADA digital camera (Olympus SIS, Münster, Germany). The sections were photographed using the Olympus TEM Imaging Platform software.

Cell culture and cytokine profiler

Human umbilical vein endothelial cells (HUVECs) were freshly isolated from human umbilical cords. Permission for cell isolations was obtained from the ethics committee of Innsbruck Medical University. Cultivation was performed in EC basal medium (Lonza, Basel, Switzerland) supplemented with EGM-2 SingleQuots supplements (Lonza). Fibroblasts were isolated from human aortic specimen and cultured in DMEM 4.5 g/l glucose (Lonza) supplemented with P/S and 10% foetal calf serum (FCS) (both Sigma, St Louis). Peripheral blood mononuclear cells (PBMCs) were isolated using Ficoll (LSM 1077 Lymphocyte, PAA, GE Healthcare, Chalfont St Giles, UK) gradient centrifugation and cultured in RPMI 1640 containing P/S and 10% FCS (all Sigma, St Louis).

To analyse cytokine changes after SWT, HUVECs were cultured in T25 flasks and treated with SW in a water bath as described previously [22]. Then 300 impulses, at an energy flux density of 0.1 mJ/mm^2 and a frequency of 3 Hz, were applied.

Cells were harvested 12 h after treatment. Protein was measured using a Pierce™ BCA Protein Assay Kit (Thermo Scientific, Waltham, MA, USA). For the evaluation of cytokine expression after SWT, a commercially available human cytokine profiler (ARY 005, R&D, Minneapolis, MN, USA) was used as recommended by the manufacturer. A total of 100 µg protein per sample was used.

Reseeding and bioreactor

Decellularized porcine aortic conduits were reseeded with HUVECs, PBMCs or fibroblasts and were cultivated under static conditions in a conventional incubator with 5% CO_2. After 24 h, reseeded conduits were exposed to pulsatile flow culture conditions using a bioreactor (CardioGen, Tissue Growth Technologies, Instron, Norwood, MA, USA). Cell-specific cell culture medium was used for the perfusion. The total perfusion time was 12 h. A pulsatility rate of 60 beats per minute at a pressure of 80/40 mmHg was applied during the entire cultivation time. SWT was applied to the reseeded cells at the beginning of the pulsatile flow cultivation (300 Impulses per conduit, at an energy flux density of 0.1 mJ/mm^2 and a frequency of 3 Hz). These SW parameters differ from the *in vivo* trial. The parameters were chosen due to the experience that SWs of lower energies are needed *in vitro* to induce a comparable response as *in vivo* [23]. Conduits were explanted 12 h after cultivation and investigated morphologically in HE staining.

Statistical analysis

Statistical comparisons between two groups were performed by unpaired Student's *t*-test using GraphPad PRISM 6 for Mac OS × (GraphPad Software, Inc., La Jolla, CA, USA). All results are expressed as mean ± SEM. *P*-values <0.05 were considered statistically significant. All experiments were repeated at least in triplicate.

RESULTS

Decellularization of grafts causes no impairment of mechanical properties

Decellularized aortas showed successful removal of cells in HE staining (data not shown). Implanted tissue-engineered heart valves need to bear strong mechanical forces within the blood stream. Therefore, as a first step, we aimed to prove that the decellularization process does not impair mechanical properties of the graft tissue. A mechanical stretch test was performed with longitudinal and transversal strips of decellularized grafts (Fig. 1A and B). The maximal force (in newton) necessary to cause rupture of the aortic strip was equal between native and decellularized samples (transversal strips native aortas 16.39 ± 1.43 N vs decellularized aortas 16.47 ± 0.69 N, $P = 0.96$; longitudinal strips native aortas 6.36 ± 0.8 N vs decellularized aortas 6.4 ± 0.71 N, $P = 0.98$) (Fig. 1C and D). For better evaluation of stiffness, the Young's modulus (=tensile modulus) was calculated in N/mm^2. Again, no differences could be observed between decellularized and native samples (transversal strips native aortas 2.824 ± 0.6210 N/mm^2 vs decellularized aortas 3.064 ± 0.2795 N/mm^2, $P = 0.73$; longitudinal strips native aortas 1.130 ± 0.2427 N/mm^2 vs decellularized aortas 1.029 ± 0.06850 N/mm^2, $P = 0.61$) (Fig. 1E and F). This clearly indicates that the decellularization process did not impair mechanical properties of the aortic grafts.

Modulation of inflammatory cytokine expression upon shock wave therapy

To analyse the impact of SW treatment on inflammation, we first measured the expression of the two key players: TNF-α and IL-6 mRNA levels via RT-PCR. Enhanced expression of TNF-α was observed in treated animals (relative gene expression: CTR 3.38 ± 0.39 vs SWT 27.26 ± 10.33, $P = 0.0498$) (Fig. 2A). In addition, IL-6 expression was increased after SWT, albeit not significantly (relative gene expression: CTR 1.62 ± 0.18 vs SWT: 2.84 ± 0.88, $P = 0.25$) (Fig. 2B). To investigate the role of SWT in macrophage recruitment and activation, cytokine levels of SW-treated HUVECs were measured using a cytokine profiler.

The pivotal macrophage recruitment factors macrophage migration inhibitory factor (MIF) and macrophage inflammatory protein 1β (MIP-1β) were up-regulated after SWT (MIF, relative protein level: CTR 0.57 ± 0.07 vs SWT 0.90 ± 0.03, $P = 0.048$;

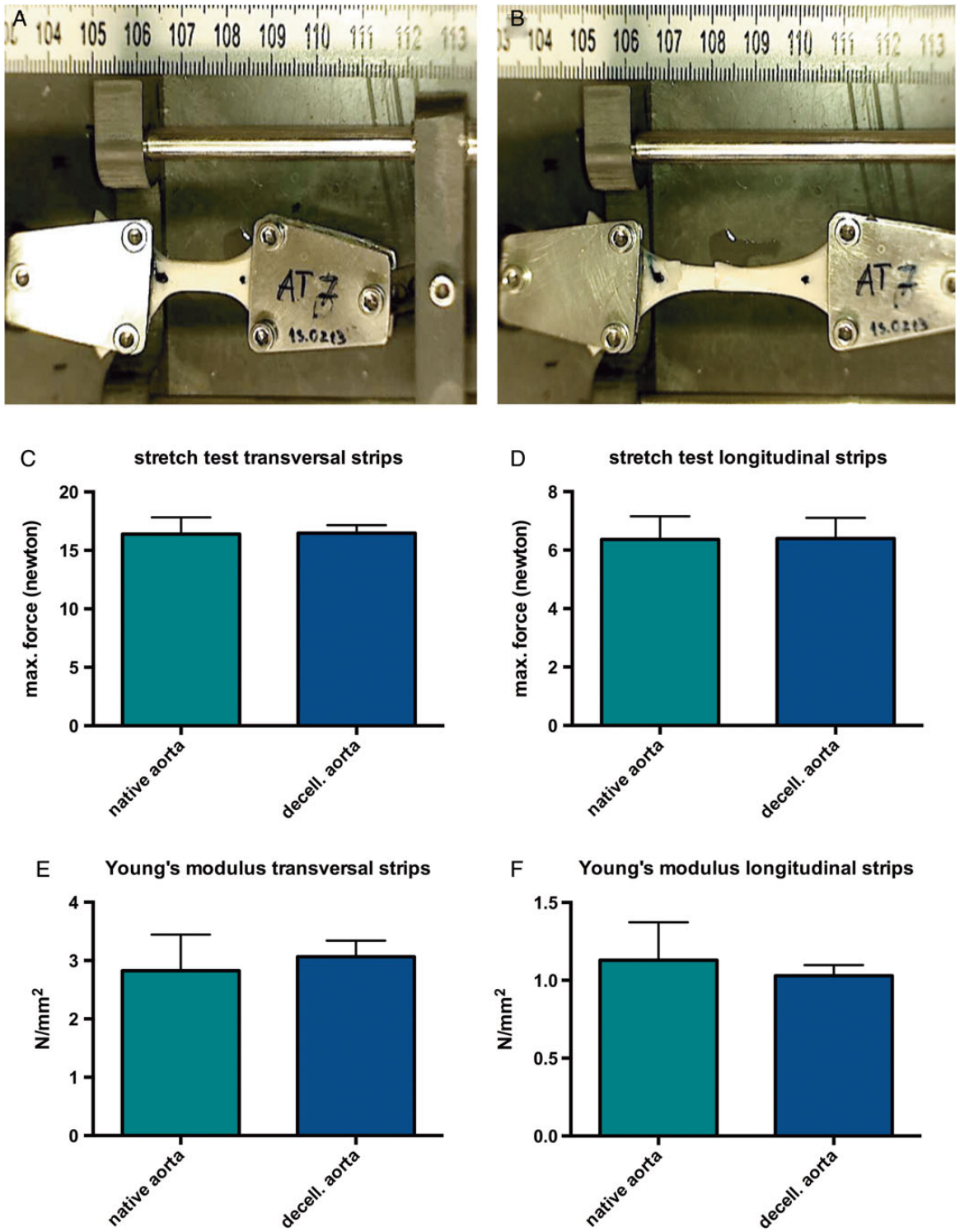

Figure 1: Decellularization causes no impairment of mechanical properties. (**A** and **B**) Representative examples of mechanically tested aortic specimens (**A**, prior to stretching; **B**, maximum stretching with beginning rupture). This experiment was performed in longitudinal and transversal strips of decellularized and native porcine aortas in order to verify their mechanical properties. A specifically designed biopsy punch was used to guarantee the exact same size among all samples. Specimens were fixed with clamps on both sides and slowly elongated with a custom-made extension machine. The force (in newton) at which rupture occurred was compared between the groups. (**C**) Comparison of rupture force of transversal strips showed no difference between native and decellularized aortas ($n = 7$). (**D**) Mechanical properties of longitudinal aortic strips showed no difference after decellularization compared with native aortas ($n = 17$). (**E**) For better evaluation of stiffness, the Young's modulus (=tensile modulus) was calculated. Transversal decellularized strips showed no significant changes compared with control strips ($n = 7$). (**F**) Decellularized longitudinal specimens showed no difference in Young's modulus compared with native controls ($n = 17$).

MIP-1β, relative protein level CTR 0.19 ± 0.02 vs SWT 0.34 ± 0.09, $P = 0.22$) (Fig. 2C and D). Levels of macrophage-activating cytokines CD40 ligand (CD40L) and complement component 5/5a (C5/C5a) were decreased after SWT (CD40L, relative protein level CTR 0.19 ± 0.02 vs SWT 0.33 ± 0.09, $P = 0.02$; C5/C5a, relative protein level CTR 0.28 ± 0.02 vs 0.13 ± 0.01, $P = 0.002$) (Fig. 2E and F). These

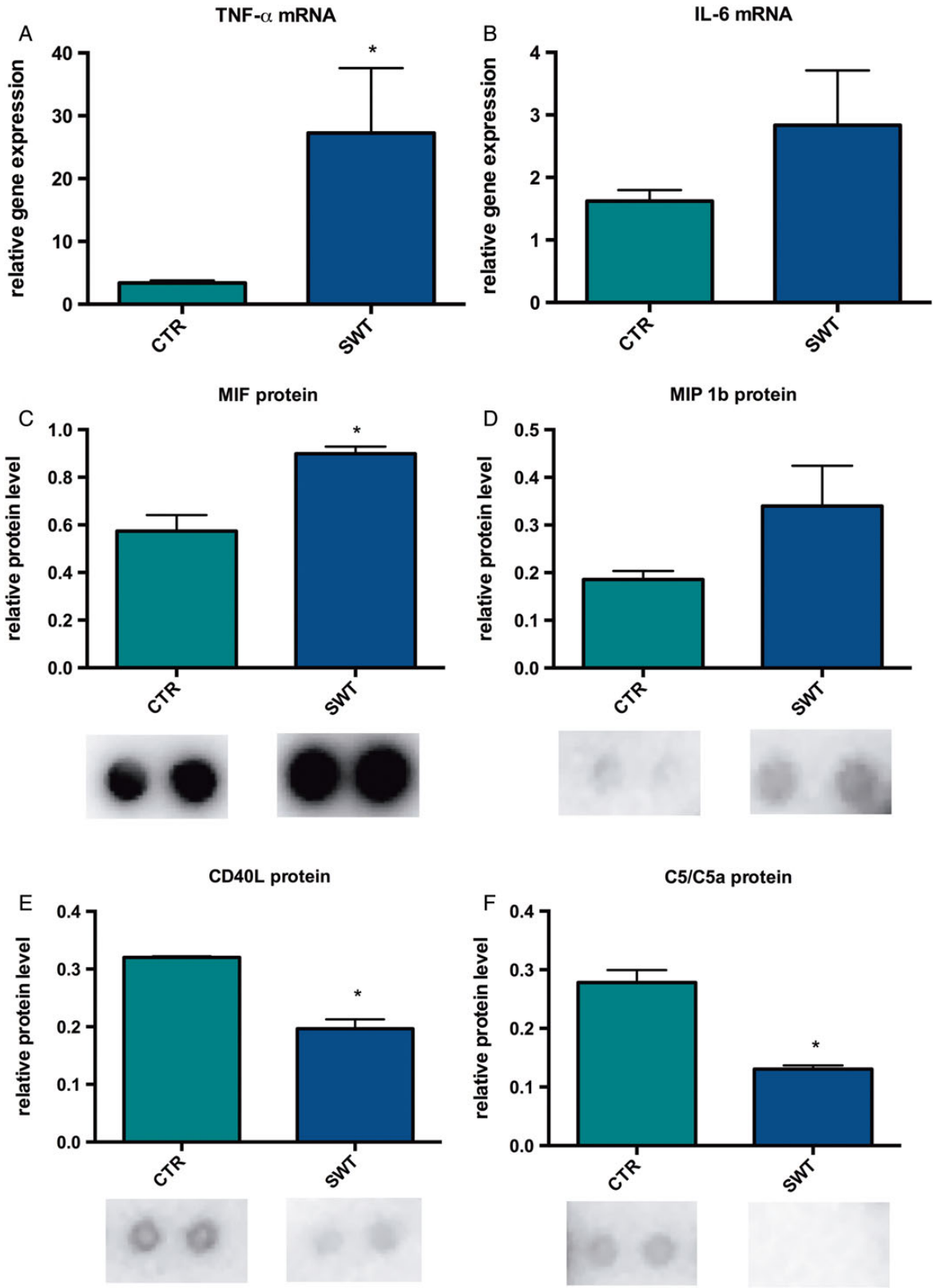

Figure 2: Modulation of inflammatory cytokine expression upon SWT. (**A**) Explanted grafts were analysed via RT-PCR for inflammatory cytokine expression. Enhanced levels of TNF-α mRNA could be observed in treated grafts ($n = 6$, $^*P < 0.05$). (**B**) SWT results in increased IL-6 expression in treated grafts ($n = 6$). (**C**) A cytokine profiler performed from HUVECs revealed after SWT, enhanced levels of macrophage MIF, which is, a pivotal macrophage recruitment factor ($^*P < 0.05$). (**D**) In line with these findings, MIP-1β was up-regulated after treatment. (**E**) SWT resulted in decreased levels of macrophage-activating protein CD40 ligand (CD40L) ($^*P < 0.05$). (**F**) Complement component 5/5a (C5/C5a), responsible for macrophage activation and polarization towards proinflammatory M1 macrophages, was down-regulated after SWT ($^*P < 0.05$). SWT: shock wave therapy; MIP-1β: macrophage inflammatory protein 1β; MIF: migration inhibitory factor; HUVECs: human umbilical vein endothelial cells; RT-PCR: reverse transcription–polymerase chain reaction; TNF-α: tumour necrosis factor α.

results give a strong hint that SWT might have an impact on macrophage recruitment and polarization towards M2 macrophages.

Shock wave therapy influences cell recruitment, macrophage polarization and graft calcification

First, explanted grafts were analysed for the invasion of recipient cells in a conventional HE staining. As grafts are acellular at the moment of implantation, cells found in the graft after harvesting can clearly be defined as recipient cells. SW-treated grafts showed a significantly increased repopulation after 72 h (number of cells per area: CTR 8.87 ± 1.13 vs SWT 13.1 ± 1.71, $P = 0.041$) and after 3 weeks (number of cells per area: CTR 15.65 ± 1.37 vs SWT 28.28 ± 4.78, $P = 0.0057$) (Fig. 3A).

F4/80 staining revealed higher numbers of macrophages 72 h (% of macrophages of total cell count: CTR 16.12 ± 2.21 vs SWT 31.31 ± 2.03, $P < 0.0001$) and three weeks after treatment (% of macrophages of total cell count: CTR 28.51 ± 3.16 vs SWT 37.60 ± 2.70, $P = 0.037$) compared with untreated controls (Fig. 3B). Interestingly, macrophages could mainly be found at the border zones of the graft (Fig. 3C). Closer characterization of the macrophage subtype via F4/80 and CD163 co-staining revealed higher numbers of M2 macrophages 3 weeks after SWT (% of total macrophages: CTR 8.71 ± 2.2 vs SWT 27.95 ± 4.14, $P = 0.0002$) (Fig. 3D). No F4/80 and CD163-positive cells could be found after 72 h (data not shown). This clearly shows that SWT influences polarization of macrophages towards their subtype M2. This is an important finding as M2 macrophages are known to positively influence tissue regeneration via several mechanisms including anti-inflammatory effects.

In a next step, we aimed to investigate whether the present macrophages interact with calcified areas. Therefore, we stained tissue sections for TRAP, a molecule that mainly disintegrates calcified extracellular matrix such as bone and cartilage and is therefore used to characterize osteoclastic cells [24]. No TRAP-positive cells could be identified 72 h after implantation (data not shown). However, 3 weeks after treatment significantly increased numbers of TRAP-positive cells were found in treated animals compared with controls (total number of TRAP-positive cells per sample: CTR 67.6 ± 14.14 vs SWT 154.6 ± 29.87, $P = 0.03$) (Fig. 3E), indicating an active osteoclastic process upon SWT. To assess whether this results in less calcification, von Kossa staining was performed. No calcifications could be identified 72 h after implantation (data not shown). However, 3 weeks after implantation, areas of calcification were decreased in treated animals compared with untreated controls (mean area of calcification in arbitrary units: CTR 1 099 000 ± 142 564 vs SWT 236 411 ± 65 388, $P = 0.0003$) (Fig. 3F).

Morphological observations

TEM analysis showed that macrophages were mainly located in the border zones of the grafts interacting with the implanted matrix. Fibroblasts invading the graft could be identified (Fig. 4A). Numerous collagen bundles could be observed in close proximity to the repopulating fibroblasts (Fig. 4B). Images in higher magnifications showed macrophages containing numerous lysosomes attached to the implanted matrix (Fig. 4C).

The overlay of serial sections of von Kossa (=calcification) and TRAP (=osteoclastic cells) stained images revealed that TRAP-positive cells are mainly located in close proximity to calcified tissue (Fig. 4D).

Behaviour of reseeded cells in a pulsatile flow perfusion system

In subcutaneously implanted grafts, we could observe repopulation with recipient cells. The largest part of them could be identified as being fibroblasts and macrophages. To analyse the behaviour of macrophages under pulsatile flow conditions, we used PBMCs, as macrophages are mainly derived from them. As the subcutaneous implantation model is limited by the fact that implanted grafts have no contact with the blood stream, ECs play a minor role in this setting. However, in a clinical setting, ECs play a pivotal role in repopulation of the graft surface. Thus, we reseeded decellularized porcine aortic conduits with fibroblasts, PBMCs or HUVECs and incubated them in a pulsatile flow bioreactor to compare coverage between the different cell types under *in vivo* conditions. Cell coverage after 12 h was measured in HE stainings. Thereby, we observed that valves repopulated with fibroblasts showed the highest amount of coverage (% of reseeded graft surface: 45.91 ± 5.52), followed by PBMCs (% of reseeded graft surface: 6.64 ± 1.08, $P < 0.0001$ vs fibroblasts) and HUVECs (% of reseeded graft surface: 1.70 ± 0.28, $P < 0.0001$ vs fibroblasts) (Fig. 5A).

As proper endothelialization after graft implantation is crucial for the avoidance of thromboembolic events in a clinical setting, we investigated whether the application of SWT would increase the coverage of HUVECs. SWT has been described to enhance cell proliferation. Analysis revealed that valves reseeded with HUVECs showed better cell coverage after SWT compared with untreated valves (% of reseeded graft surface: CTR 1.70 ± 0.28 vs SWT 4.85 ± 0.87; $P = 0.0005$) (Fig. 5B).

DISCUSSION

Tissue engineering represents a promising approach to overcome the limitations of glutaraldehyde-fixed bioprosthetic heart valves, which are mainly progressive tissue degeneration and the lack of ability to grow and repair [2]. Decellularized allografts have been successfully implanted in children undergoing surgical valve replacement and showed satisfying long-term results [7]. However, as the availability of allografts is limited, there is a need for research on alternative tissue sources. The use of xenografts is a promising option. However, xenografts can cause a massive inflammatory response leading to graft failure [11]. Current approaches to overcome this problem and prolong graft survival include reseeding of decellularized grafts with recipient cells prior to implantation. However, complete coverage and thereby avoiding immune response remains challenging.

SWs have been extensively described to modulate inflammation and enhance re-epithelialization in cutaneous burn wounds [17, 18]. In the current study, we therefore aimed to investigate whether (i) SW treatment may lead to decreased calcification of subcutaneously implanted porcine xenografts in mice and (ii) endothelialization of decellularized aortic valve conduits under pulsatile flow conditions may be improved.

In a first step, decellularized porcine aortic strips were tested for their mechanical properties and compared with native tissue in order to exclude major alteration by the decellularization process. No difference was observed between native and decellularized

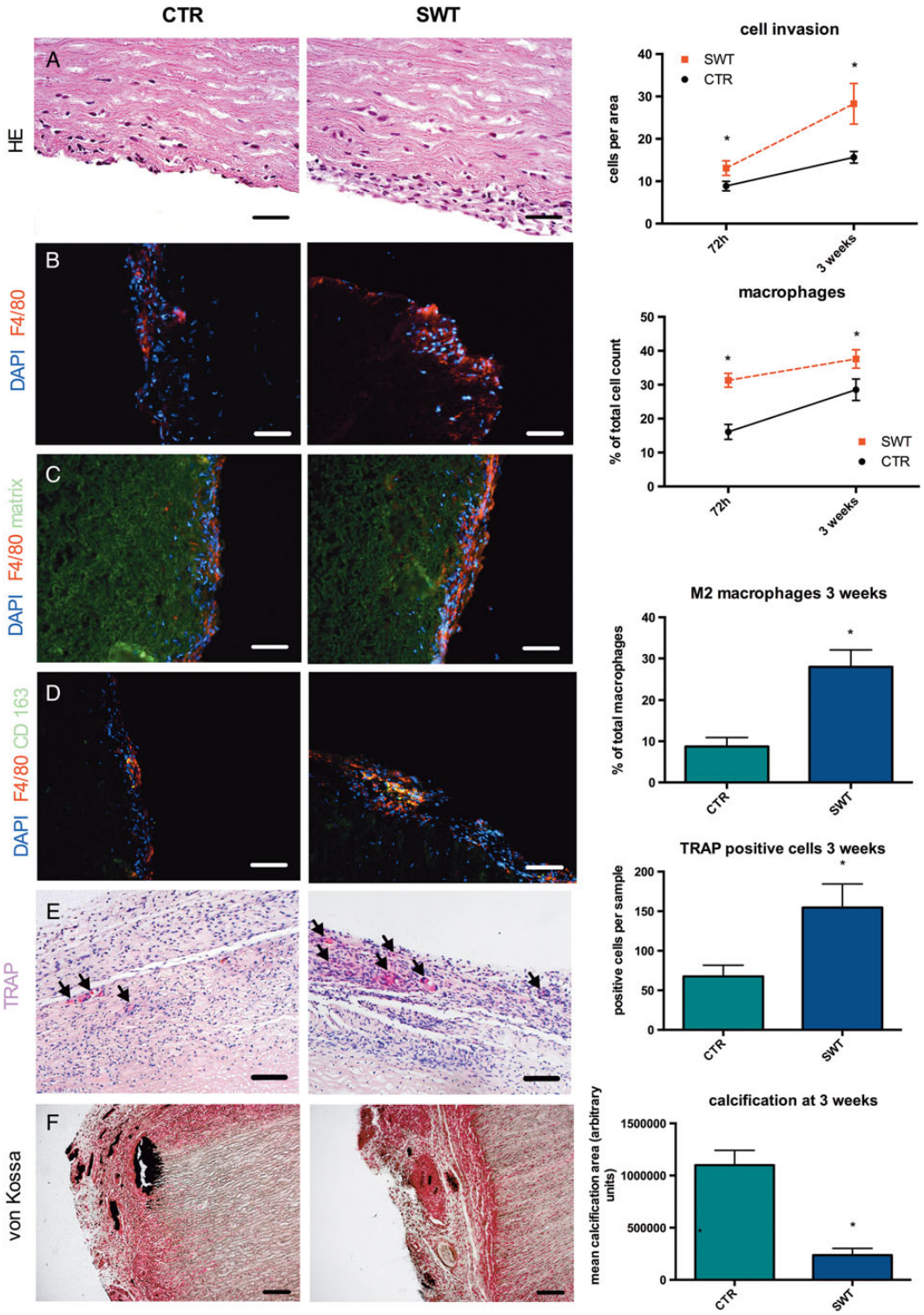

Figure 3: SWT influences cell recruitment, macrophage polarization and graft calcification. Images depict representative samples from treated grafts and control grafts 3 weeks after treatment. (**A**) After harvesting, cells were counted in a conventional HE staining. As grafts are acellular at the moment of implantation, visualized cells can be defined as recipient cells. Grafts exhibit significantly increased numbers of repopulating cells 72 h after SWT compared with untreated controls. Three weeks after SWT, treated grafts still show enhanced repopulation compared with untreated controls (scale bar: 50 µm, $n = 6$, $^*P < 0.05$). (**B**) Immunofluorescence staining for total macrophages (F4/80) was performed. SWT results in enhanced macrophage (red) recruitment 72 h and 3 weeks after treatment (scale bar: 100 µm, red = F4/80, blue = DAPI, $n = 6$, $^*P < 0.05$). (**C**) Macrophages (red) were mainly found at the border zones of the graft, indicating that they might digest the matrix. Long exposure was utilized to visualize the implanted graft by its autofluorescence (green) (scale bar: 100 µm, red = F4/80, blue = DAPI). (**D**) Treated grafts showed higher infiltration with M2 macrophages identified by F4/80 and CD163 double staining 3 weeks after treatment (scale bar: 100 µm, red = F4/80, blue = DAPI, green = CD163, $n = 6$, $^*P < 0.05$). (**E**) Explanted grafts were stained for the osteoclastic enzyme TRAPa molecule that disintegrates calcified extracellular matrix. Quantification of TRAP-positive cells (pink, arrow heads) showed increased numbers of cells with osteoclastic activity 3 weeks after treatment compared with untreated controls (scale bar: 100 µm, $n = 6$, $^*P < 0.05$). (**F**) To assess graft degeneration, specimens were analysed for calcifications using von Kossa staining. Decreased areas of calcification (black) 3 weeks after SWT could be observed in the treatment group compared with controls (scale bar: 200 µm, $n = 6$, $^*P < 0.05$). SWT: shock wave therapy; TRAP: tartrate-resistant acid phosphatase; DAPI: 4′,6-diamidino-2-phenylindole; HE: haematoxylin–eosin.

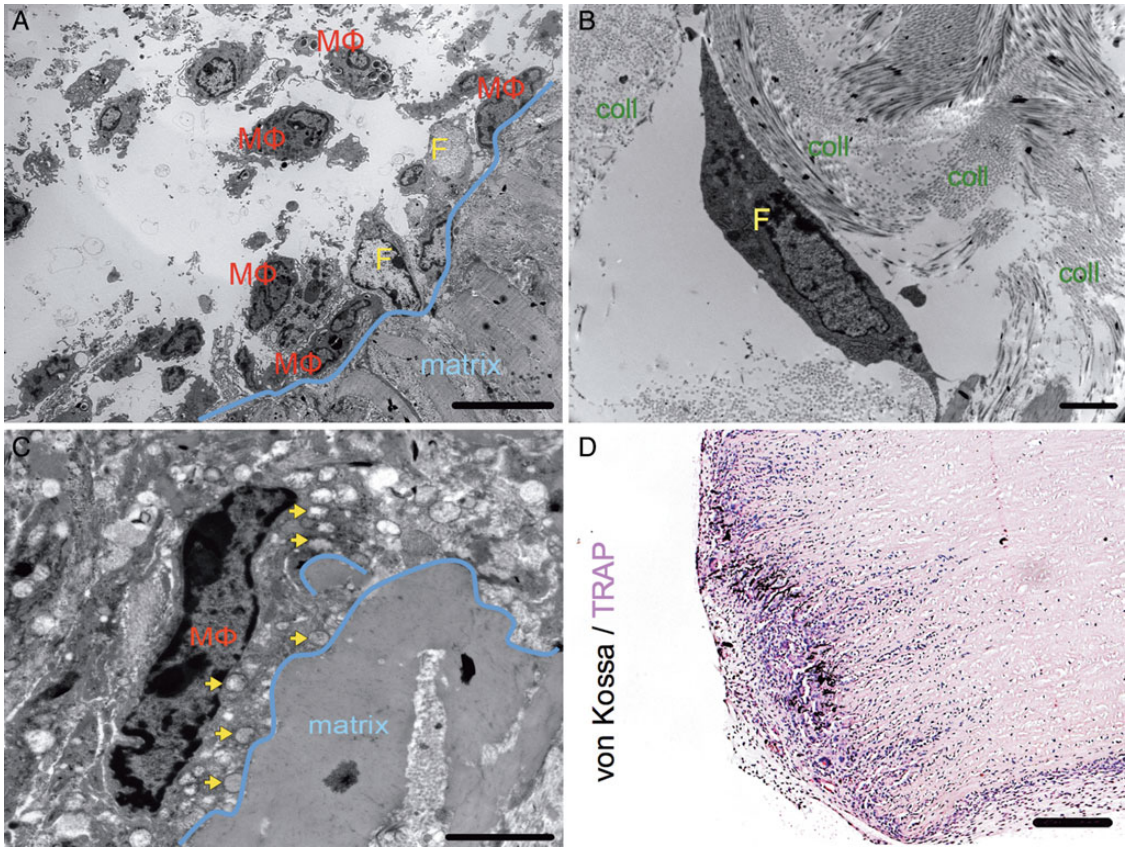

Figure 4: Morphological observations. (**A**) TEM images show that macrophages are mainly located at the border zone and might disintegrate the implanted matrix in preparation for fibroblast invasion (scale bar: 10 µm, Mϕ = macrophage, F = fibroblast). (**B**) Invaded fibroblasts show high amounts of collagen in their proximity. This could be due to collagen production within the implanted matrix by recipient cells. However, it is not possible to distinguish between collagen bundles produced by the invading cells and collagen originating from the implanted matrix (scale bar: 2 µm, F = fibroblast, coll = collagen). (**C**) Macrophages containing numerous lysosomes are attached to the implanted matrix (scale bar: 2 µm, Mϕ = macrophage, arrow heads = lysosomes). (**D**) To assess whether TRAP-positive cells interact with calcifications, an overlay of serial sections from stainings for calcification (von Kossa) and osteoclastic cells (TRAP) was performed. TRAP-positive cells (pink) can mainly be observed in close proximity to calcified areas (black) of the graft (scale bar: 100 µm). TRAP: tartrate-resistant acid phosphatase; TEM: transmission electron microscopy.

tissue. This result is consistent with the findings published by Lichtenberg *et al.* elsewhere [6]. Thus, it seems that the main factors responsible for the mechanical strength are contributed by the extracellular matrix.

In a model of subcutaneous xenograft implantation in mice, we show that SW-treated animals exhibit increased cell repopulation of the implanted graft. Additionally, higher numbers of macrophages after SW treatment were found in the border zone of the grafts. TEM pictures reveal macrophages containing lysosomal vesicles attached to the matrix. We therefore suggest that macrophages could digest the implanted matrix and thereby enable the invasion of other cell types into the graft. As such, mainly fibroblasts could be observed in TEM images. However, this mere observation needs to be clarified in future mechanistic experiments.

In line with these findings, TNF-α and IL-6 mRNA expression were increased in the SWT group, although this was not significant for IL-6. Interestingly, the fold increase of TNF-α was much higher than the fold increase in IL-6 after SWT. Both cytokines are not only known to recruit macrophages, but are also produced by macrophages [13, 14]. Moreover, we found higher protein levels of the pivotal macrophage recruitment factors MIF and MIP-1β after SWT therapy. This up-regulation could be responsible for the increased macrophage recruitment after treatment.

Closer characterization of the macrophage subtypes revealed higher numbers of M2 macrophages related to the total number of macrophages after SWT. M2 macrophages are known to be crucial for matrix turnover and remodelling. Obviously, SWT causes macrophage polarization towards M2. CD40L and C5/C5a have been described to activate macrophages and to promote the polarization towards proinflammatory M1 macrophages. In line with the other findings, we found decreased levels of CD40L and C5/C5a after SWT.

Moreover, we show in TRAP stainings that some of the recruited cells show osteoclastic activity. These cells were found in close proximity to calcified tissue and significantly more of them upon SWT. TRAP-positive cells have been found in calcific atherosclerotic lesions [25]. To the best of our knowledge, this is the first time that involvement of osteoclastic cells in the infiltration of decellularized grafts has been observed.

In addition, we found smaller areas of calcifications after SWT. The exact mechanisms of xenograft degeneration remain largely unknown. It has been shown that remaining epitopes like the alpha-gal epitope trigger immune reactions leading to graft failure. It remains unclear how immune responses lead to calcification. However, we think that therapies that modulate the acute inflammatory response and thereby delay or even diminish chronic

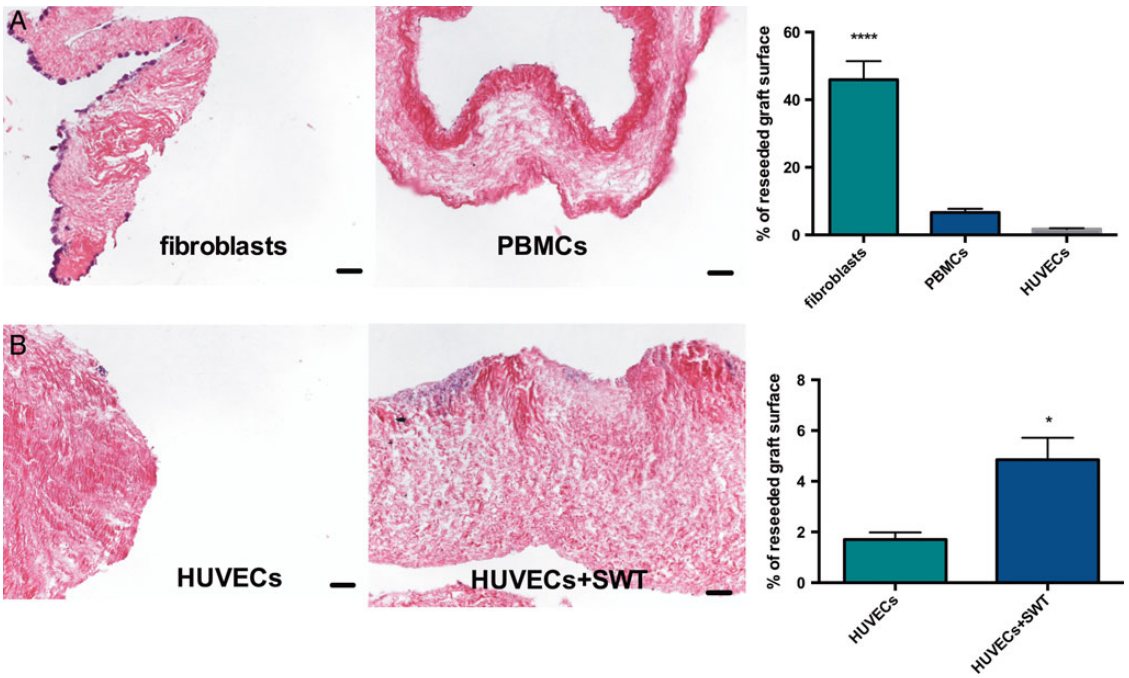

Figure 5: Cell coverage of decellularized grafts under pulsatile flow conditions. (**A**) Decellularized porcine aortic valve conduits were reseeded with HUVECs, fibroblasts or PBMCs and put in a pulsatile flow perfusion system. After 12 h, coverage was analysed. Fibroblasts showed better coverage performance compared with PBMCs and HUVECs (scale bar: 100 µm, $n = 6$, ****$P < 0.0001$ versus both the other groups). (**B**) As insufficient repopulation with recipient cells prior to implantation represents a major challenge in tissue engineering, we investigated whether SWT could improve coverage of endothelial cells. In fact, SW treatment of HUVECs resulted in significantly improved coverage compared with untreated controls (scale bar: 100 µm, $n = 6$, *$P < 0.05$). SW: shock wave; SWT: shock wave therapy; HUVECs: human umbilical vein endothelial cells; PBMCs: peripheral blood mononuclear cells.

inflammation might develop as a feasible adjunct to the treatment of decellularized xenografts when implanted.

To evaluate cells under *in vivo* conditions, a pulsatile perfusion bioreactor was used and decellularized aortic valve conduits were repopulated with fibroblasts, PBMCs or ECs prior to exposure. With this experiment, we aimed to investigate which cell type performs best for prosthesis coverage. Fibroblasts clearly showed the best coverage, followed by PBMCs and ECs. These results indicate that fibroblasts are crucial in the first hours of repopulation of the graft under pulsatile flow conditions. Additionally, they may play an important role in the early inflammatory response to xenograft tissue. However, proper endothelialization is crucial for the avoidance of immune reactions and thromboembolic events [3]. SWs have been described to induce cell proliferation [23]. We therefore further investigated whether the application of SWs would have a positive impact on aortic valve repopulation by ECs and found that treated cells indeed showed an increase in total coverage area in a bioreactor system.

In summary SWs modulate the acute inflammatory response to xenograft implantation and thereby decrease later calcification. Moreover, endothelialization of grafts under pulsatile flow conditions is increased. SW treatment could therefore develop as a feasible adjunct to heart valve tissue engineering.

Limitations

Pieces of decellularized porcine aortic wall were subcutaneously implanted in mice. Although we think that the response to the xenografts is mainly dependent on the decellularization protocol, our results need to be verified with decellularized valve tissue in future experiments as well as in bloodstream perfusion. Moreover, merging TRAP and von Kossa stainings of serial sections had to be used as an auxillary method, as it is technically impossible to perform both stainings on one slide. This method is not as accurate as double-staining would be.

Coverage of the reseeded conduits was assessed 12 h after SWT. Therefore, knowledge about the long-term effect of SWT is still missing and has to be addressed in future experiments.

ACKNOWLEDGEMENTS

We kindly thank Annabella Knab and Katharina Heinz for performing tissue sections and Gerhard Moser for helping with calculation of the Young's modulus.

Funding

This work was in part supported by a research grant of Medizinischer Forschungsfonds Tirol (MFF) (project no. 220) and by a research grant provided by TRT—Tissue Regeneration Technologies LLC, Woodstock, GA, USA, both to Johannes Holfeld.

Conflict of interest: none declared.

REFERENCES

[1] Cannegieter SC, Rosendaal FR, Briet E. Thromboembolic and bleeding complications in patients with mechanical heart valve prostheses. Circulation 1994;89:635–41.
[2] El Oakley R, Kleine P, Bach DS. Choice of prosthetic heart valve in today's practice. Circulation 2008;117:253–6.
[3] Schoen FJ. Evolving concepts of cardiac valve dynamics: the continuum of development, functional structure, pathobiology, and tissue engineering. Circulation 2008;118:1864–80.

[4] Schoen FJ. Heart valve tissue engineering: quo vadis? Curr Opin Biotechnol 2011;22:698–705.

[5] Hoerstrup SP, Kadner A, Melnitchouk S, Trojan A, Eid K, Tracy J *et al*. Tissue engineering of functional trileaflet heart valves from human marrow stromal cells. Circulation 2002;106:I143–50.

[6] Lichtenberg A, Tudorache I, Cebotari S, Ringes-Lichtenberg S, Sturz G, Hoeffler K *et al*. In vitro re-endothelialization of detergent decellularized heart valves under simulated physiological dynamic conditions. Biomaterials 2006;27:4221–9.

[7] Cebotari S, Tudorache I, Ciubotaru A, Boethig D, Sarikouch S, Goerler A *et al*. Use of fresh decellularized allografts for pulmonary valve replacement may reduce the reoperation rate in children and young adults: early report. Circulation 2011;124:S115–23.

[8] Rieder E, Seebacher G, Kasimir MT, Eichmair E, Winter B, Dekan B *et al*. Tissue engineering of heart valves: decellularized porcine and human valve scaffolds differ importantly in residual potential to attract monocytic cells. Circulation 2005;111:2792–7.

[9] Erdbrugger W, Konertz W, Dohmen PM, Posner S, Ellerbrok H, Brodde OE *et al*. Decellularized xenogenic heart valves reveal remodeling and growth potential in vivo. Tissue Eng 2006;12:2059–68.

[10] Konertz W, Dohmen PM, Liu J, Beholz S, Dushe S, Posner S *et al*. Hemodynamic characteristics of the Matrix P decellularized xenograft for pulmonary valve replacement during the Ross operation. J Heart Valve Dis 2005;14:78–81.

[11] Simon P, Kasimir MT, Seebacher G, Weigel G, Ullrich R, Salzer-Muhar U *et al*. Early failure of the tissue engineered porcine heart valve SYNERGRAFT in pediatric patients. Eur J Cardiothorac Surg 2003;23: 1002–6; discussion 06.

[12] Brown BN, Valentin JE, Stewart-Akers AM, McCabe GP, Badylak SF. Macrophage phenotype and remodeling outcomes in response to biologic scaffolds with and without a cellular component. Biomaterials 2009; 30:1482–91.

[13] Lo SZ, Steer JH, Joyce DA. Tumor necrosis factor-alpha promotes survival in methotrexate-exposed macrophages by an NF-kappaB-dependent pathway. Arthritis Res Ther 2011;13:R24.

[14] Zhang C, Li Y, Wu Y, Wang L, Wang X, Du J. Interleukin-6/signal transducer and activator of transcription 3 (STAT3) pathway is essential for macrophage infiltration and myoblast proliferation during muscle regeneration. J Biol Chem 2013;288:1489–99.

[15] Macchiarini P, Jungebluth P, Go T, Asnaghi MA, Rees LE, Cogan TA *et al*. Clinical transplantation of a tissue-engineered airway. Lancet 2008;372: 2023–30.

[16] Ottomann C, Hartmann B, Tyler J, Maier H, Thiele R, Schaden W *et al*. Prospective randomized trial of accelerated re-epithelization of skin graft donor sites using extracorporeal shock wave therapy. J Am Coll Surg 2010; 211:361–7.

[17] Ottomann C, Stojadinovic A, Lavin PT, Gannon FH, Heggeness MH, Thiele R *et al*. Prospective randomized phase II Trial of accelerated reepithelialization of superficial second-degree burn wounds using extracorporeal shock wave therapy. Ann Surg 2012;255:23–9.

[18] Davis TA, Stojadinovic A, Anam K, Amare M, Naik S, Peoples GE *et al*. Extracorporeal shock wave therapy suppresses the early proinflammatory immune response to a severe cutaneous burn injury. Int Wound J 2009;6: 11–21.

[19] Aicher A, Heeschen C, Sasaki K, Urbich C, Zeiher AM, Dimmeler S. Low-energy shock wave for enhancing recruitment of endothelial progenitor cells: a new modality to increase efficacy of cell therapy in chronic hind limb ischemia. Circulation 2006;114:2823–30.

[20] Lorusso R, Corradi D, Maestri R, Bosio S, Curulli A, Beghi C *et al*. Atorvastatin attenuates post-implant tissue degeneration of cardiac prosthetic valve bovine pericardial tissue in a subcutaneous animal model. Int J Cardiol 2010;141:68–74.

[21] Tepekoylu C, Wang FS, Kozaryn R, Albrecht-Schgoer K, Theurl M, Schaden W *et al*. Shock wave treatment induces angiogenesis and mobilizes endogenous CD31/CD34-positive endothelial cells in a hindlimb ischemia model: implications for angiogenesis and vasculogenesis. J Thorac Cardiovasc Surg 2013;146:971–8.

[22] Holfeld J, Tepeköylü C, Kozaryn R, Mathes W, Grimm M, Paulus P. Shock wave application to cell cultures. J Vis Exp. 2014;(86).

[23] Weihs AM, Fuchs C, Teuschl AH, Hartinger J, Slezak P, Mittermayr R *et al*. Shock wave treatment enhances cell proliferation and improves wound healing by ATP release-coupled extracellular signal-regulated kinase (ERK) activation. J Biol Chem 2014;289:27090–104.

[24] Hayman AR. Tartrate-resistant acid phosphatase (TRAP) and the osteoclast/immune cell dichotomy. Autoimmunity 2008;41:218–23.

[25] Demer L, Tintut Y. The roles of lipid oxidation products and receptor activator of nuclear factor-kappaB signaling in atherosclerotic calcification. Circ Res 2011;108:1482–93.